Journal of The Electrochemical Society, **164** (4) E53-E61 (2017)
0013-4651/2017/164(4)/E53/9/$37.00 © The Electrochemical Society

Effective Ion Diffusion in Charged Nanoporous Materials

Xuan Zhang[a] and Daniel M. Tartakovsky[b,z]

[a]*Department of Mechanical and Aerospace Engineering, University of California, San Diego, La Jolla, California 92093, USA*
[b]*Department of Energy Resources Engineering, Stanford University, Stanford, California 94305, USA*

Multiscale models of ion transport in porous media relate microscopic material properties (e.g., pore size distribution and pore connectivity) to their macroscopic counterparts (e.g., porosity, effective diffusion coefficient and effective electrical conductivity). We derive a macroscopic model of ion transport in electrically charged nanoporous materials, and the corresponding effective diffusion coefficient, electric conductivity and transference numbers, that explicitly account for dynamic changes in electrical double layer (EDL) and possible overlap of EDLs in nanopores. The general equations comprising this model reduce to a model of an electrical double layer capacitor (EDLC) used to interpret measurements of the EDLC voltage response to charging. While the original representation relies on empirical coefficients (e.g., Bruggeman's relation), our effective coefficients are derived from the first principles and vary with a range of electrochemical conditions (e.g., initial concentration of ions in the electrolyte). The resulting model predictions of the EDLC voltage response match the experimental data better than the original model does.

Manuscript submitted November 28, 2016; revised manuscript received January 11, 2017. Published February 2, 2017.

Rapid growth of the global economy, depletion of fossil fuels, and increasing environmental concerns accelerate the shift to renewable (e.g., solar and wind) energy production and electric and/or hybrid electric vehicles with low CO_2 emissions. These and other applications rely on energy conversion and storage technologies. Some of the most effective and practical technologies for electrochemical energy conversion and storage are batteries, fuel cells, and electrochemical supercapacitors. Their performance needs to substantially improve in order to meet power density and energy density demands. This requires breakthroughs in our understanding of electrochemical phenomena at the nanoscale and ability to model these processes at the device scale, and parlaying them into design of new materials and devices.

Nanoscale pore-structure of, e.g., electrodes affects energy storage through formation of electrical double layer (EDL) at the solid material/electrolyte interfaces.[1–5] EDL formation also plays an important role in other physical, chemical and biological systems, including separation processes used to remove heavy metals from aqueous solutions, groundwater remediation mediated by electrosorption, and capacitive desalination.[6]

Nanoporous materials with a hierarchical porous structure are thought to possess attractive electrosorption and capacitance characteristics due to their large specific surface area (provided by mircropores) and fast transport (facilitated by mesopores).[7] However, their large surface areas do not always translate into more energy stored on the surface, because the local electrical potential formation can both dominate ion transport and sorption inside nanopores and restrict pore accessibility. For example, poor electrochemical accessibility of micropores was found to significantly reduce the extent of surface reactions between the electrode material and electrolyte.[8,9] This suggests that porous structure of a nanoporous material controls power density and accessibility to the energy stored on the interface.

Qualitative understanding and quantitative predictions of this phenomenon and, more specifically, the effects of EDL on ion transport are a prerequisite for bottom-up design of new nanoporous metamaterials.[10] Guided by the goal of maximizing an electrode's specific surface area accessible to electrolyte, an optimal design of such materials must account for the potential overlap of EDLs in nanoporous structures saturated with a very dilute solution, which decreases not only the ion transport rate but also the equilibrium concentration of ions inside the pores. Such design strategies are guided by mathematical models that relate microscopic material properties (e.g., pore size distribution and pore connectivity) to their macroscopic counterparts (e.g., porosity, effective diffusion coefficient and effective electrical conductivity).

A commonly used approach is to postulate the equivalency of mathematical descriptors on the pore and continuum scales and to use phenomenological relations to express coefficients of the continuum-scale equations in terms of their pore-scale counterparts. For instance, a diffusion process taking place within the pore network of a porous electrode might be described by diffusion equations at both scales, and the molecular diffusion coefficient D in the pore-scale equation is replaced at the continuum scale with an assumed effective diffusion coefficient $D^{\text{eff}} = \omega D/\tau$, where ω and τ are the material's porosity and tortuosity, respectively, often supplemented with Bruggeman's relation[11] $\tau = \omega^{-1/2}$. This widely-used expression for estimation of effective properties in electrochemical systems is thought to be applicable for materials with low porosity, connected electrolyte transport paths, and spherical electrode particles.[12] Many porous electrode metamaterials and local electrical conditions (electrolyte concentration and applied electric field) do not satisfy these conditions, undermining the veracity of the Bruggeman model (as we demonstrate in this study) or, at least, the value of its exponent.[11,13]

Derivation of more rigorous models often relies on homogenization, e.g., via multiple-scale expansions. For example, it was used to derive macroscopic Poisson-Nernst-Planck (PNP) equations under assumptions of either a fixed surface charge density on the solid matrix[14] or an infinitely thin EDL;[15] to obtain macroscopic Onsager's reciprocal relations from a linearized version of PNP equations;[16] and to derive a macroscopic PNP-based model of water flow and ion transport in geological deformable porous media.[17–20] In addition to providing a map between the microscopic and macroscopic parameters and processes, homogenization establishes both the rigorous macroscopic descriptors grounded in the first principles and the limits of applicability of macroscopic models.[21] The homogenization analyses mentioned above are grounded in physical limitations: the assumption of a fixed surface charge density translates into an upscaled Poisson equation that does not contain information about the local electric potential distribution[14] and is not applicable for electrochemical processes in which zeta potential and solution concentration change in response to charging/discharging.[19,20]

In contrast to these and other similar studies (e.g., Ref. 22) we derive a macroscopic model of ion transport in electrically charged nanoporous materials, and the corresponding effective diffusion coefficient, electric conductivity and transference numbers, that explicitly account for dynamic changes in the EDL. Our model goes beyond the infinitely thin EDL approximation and, hence, accounts for possible overlap of EDLs in nanopores. The general equations comprising this model reduce to a model of an electrical double layer capacitor (EDLC) used to interpret measurements of the EDLC voltage response to charging.[23] While the original model[23] relies on empirical coefficients, such as $D^{\text{eff}} = \omega D/\tau$ or its Bruggeman's analog $D^{\text{eff}} = \omega^{3/2} D$, our effective coefficients are derived from the first principles and vary with electrochemical conditions (e.g., initial concentration of ions in the electrolyte). The resulting model predictions of the EDLC voltage

[z]E-mail: tartakovsky@stanford.edu

response match the experimental data[23] better than the original model did.

Problem Description

We consider a hierarchical porous material Ω with a characteristic length L. Let $\mathcal{P}$ denote the part of this material occupied by nanopores whose characteristic length scale, e.g., a typical pore diameter, is l such that $\epsilon \equiv l/L \ll 1$. The impermeable solid skeleton $\mathcal{S}$ occupies the rest of the nanoporous material, i.e., $\Omega = \mathcal{P} \cup \mathcal{S}$. The (multi-connected, smooth) boundary between the pore space $\mathcal{P}$ and the solid skeleton $\mathcal{S}$ is denoted by Γ.

The pore space $\mathcal{P}$ is completely occupied by an ionized fluid, in which cations and anions have concentrations $c_+(\mathbf{x}, t)$ and $c_-(\mathbf{x}, t)$, respectively; these concentrations have units [mol/L^3], and vary both in space, $\mathbf{x} \in \mathcal{P}$, and time t. Interactions between the ionized solution and static charges at the solid-fluid interface Γ give rise to an electrical double layer.

Microscopic models of ion transport through the hierarchical porous material Ω track the spatiotemporal evolution of $c_\pm(\mathbf{x}, t)$ inside a complex pore network $\mathcal{P}$; they rest on a solid electrochemical foundation but are computationally demanding, and often prohibitively so. Macroscopic models treat the porous material Ω as a continuum, i.e., associate ion concentrations $C_\pm(\mathbf{x}, t)$ with a certain (representative elementary) volume of the material, over which the pore-scale concentrations $c_\pm(\mathbf{x}, t)$ are averaged; such models are largely phenomenological, but relatively fast to solve. Microscopic and macroscopic formulations are provided below. Establishing the relationship between the two is one of the main goals of this study.

Microscopic transport model.—*Processes in the fluid-filled pores* $\mathcal{P}$.—We adopt the dilute theory of solvents, which treats ions as point charges and defines electrochemical potential [J/mol] as $\mu_\pm = \bar{\mu}_\pm + RT \ln c_\pm + z_\pm F \varphi$ where $\bar{\mu}_\pm$ is a reference value, and $z_\pm$ are the ion charges (valencies) [−]. Here R [J/K/mol] and F [C/mol] are the gas and Faraday constants, respectively; T [K] is temperature; and φ [V] is the electric potential. Spatial variability of $\mu_\pm$ induces ionic (Nernst-Planck) fluxes $\mathbf{J}^\pm_{\mathrm{NP}} = -M_\pm c_\pm \nabla \mu_\pm$, where the ion mobility $M_\pm$ is related to the molecular diffusion coefficient of ions in the fluid, $\mathcal{D}_\pm$ [L^2/T], by the Einstein relation $M_\pm = \mathcal{D}_\pm/RT$. In the absence of homogeneous chemical reactions, mass conservation of anions and cations, $\partial_t c_\pm = -\nabla \cdot \mathbf{J}^\pm_{\mathrm{NP}}$, gives rise to the Nernst-Planck equations

$$\frac{\partial c_\pm}{\partial t} = \nabla \cdot [\mathcal{D}_\pm(\nabla c_\pm + c_\pm \frac{z_\pm F}{RT} \nabla \varphi)], \qquad \mathbf{x} \in \mathcal{P}. \tag{1}$$

The total (net) ionic charge density $q \equiv F(z_+c_+ + z_-c_-)$ is related to the electric potential $\varphi(\mathbf{x}, t)$ through a Poisson equation,

$$-\mathcal{E}\nabla^2\varphi = F(z_+c_+ + z_-c_-), \qquad \mathbf{x} \in \mathcal{P}, \tag{2}$$

where $\mathcal{E}$ is dielectric constant of the solvent.

Processes on the fluid-solid interface Γ.—Within the electrical double layer (EDL) framework, the electrically charged surface Γ is "coated" with a compact Stern layer comprised of mixture of solvent molecules and a single layer of adsorbed ions. These are effectively immobilized by the interplay of adsorption, van der Waals forces and hydrogen bonding. To simplify the presentation, we assume the thickness of the Stern layer, $\ell_S \sim 0.03$ nm to 0.2 nm (a typical diameter of an ion)[24] to be negligible relative to the characteristic pore size $\ell_p \sim 1.0$ nm (a typical diameter of a micropore) to 25.0 nm (that of a mesopore), so that the Nernst-Planck-Poisson (PNP) Equations 1–2 are defined on the whole domain $\mathcal{P}$ and the corresponding boundary conditions are specified on the fluid-solid interface Γ. (The analysis presented below is valid even when this assumption does not hold, in which case the transport domain $\mathcal{P}$ is reduced by the thickness of the Stern layer to $\mathcal{P}_-$ and the interface Γ is replaced with Γ_-, the surface of $\mathcal{P}_-$.)

Following the standard practice,[25,26] we assume that the surface Γ carries a constant electric (zeta) potential φ_Γ, which translates into a Dirichlet boundary condition

$$\varphi(\mathbf{x}, t) = \varphi_\Gamma, \quad \mathbf{x} \in \Gamma. \tag{3}$$

This assumption is applicable if the solid matrix $\mathcal{S}$ is highly conductive, which occurs, e.g., in carbon aerogels[27]. Heterogeneous chemical reactions, $f_\pm(c_-, c_+)$, at the fluid-solid interface Γ, give rise to Robin boundary conditions

$$-\mathbf{n} \cdot \mathcal{D}_\pm(\nabla c_\pm + c_\pm \frac{z_\pm F}{RT} \nabla \varphi) = f_\pm(c_-, c_+), \qquad \mathbf{x} \in \Gamma. \tag{4}$$

When the EDL is stably formed, the situation considered in the present analysis, the surface electrosorption reaction reaches equilibrium, $f_\pm \equiv 0$. This implies the absence of the net local current source.

EDL-explicit decomposition.—The remaining part of the EDL consists of a diffusive layer, in which the EDL potential $\varphi_{\mathrm{EDL}}(\mathbf{x}, t)$ decays rapidly with the distance from the charged surface Γ. Depending on a pore's size, this diffusive layer can either occupy the entire pore space or coexist with an electrically neutral ($c_+/\nu_+ = c_-/\nu_- \equiv c_\mathrm{b}$, where $\nu_\pm$ are the dissociation coefficients) bulk electrolyte[6] present in the pore's core. This suggests a decomposition of the unknown electric potential $\varphi(\mathbf{x}, t)$ into the sum[28]

$$\varphi = \varphi_{\mathrm{EDL}} + \varphi_\mathrm{b}. \tag{5}$$

It follows from Eq. 2 and the electroneutrality condition that the bulk electric potential $\varphi_\mathrm{b}(\mathbf{x}, t)$ satisfies

$$\nabla^2\varphi_\mathrm{b} = 0, \quad \mathbf{x} \in \mathcal{P}; \qquad \varphi_\mathrm{b} = 0, \quad \mathbf{x} \in \Gamma; \tag{6}$$

and is driven by an externally imposed (macroscopic) potential gradient.

Thermodynamic equilibrium between the EDL and electrolyte's core requires the equality of their respective chemical potentials $\mu_\pm$ and $\mu_{\mathrm{b}\pm}$. Recalling the definition of chemical potential, this yields $z_\pm F\varphi + RT \ln c_\pm = z_\pm F\varphi_\mathrm{b} + \nu_\pm RT \ln c_\mathrm{b}$. Combining this with the decomposition in Eq. 5 yields a Boltzmann distribution for ion concentrations in the EDL,

$$c_\pm = \nu_\pm c_\mathrm{b} \exp\left(-\frac{z_\pm F}{RT}\varphi_{\mathrm{EDL}}\right). \tag{7}$$

Relations 5 and 7 transform dependent variables $\varphi(\mathbf{x}, t)$, $c_+(\mathbf{x}, t)$ and $c_-(\mathbf{x}, t)$ into new unknowns $\varphi_{\mathrm{EDL}}(\mathbf{x}, t)$, $\varphi_\mathrm{b}(\mathbf{x}, t)$ and $c_\mathrm{b}(\mathbf{x}, t)$. Substituting these relations into Eqs. 1 and 4 gives transformed Nernst-Planck equations

$$\frac{\partial}{\partial t}\left(c_\mathrm{b} e^{-\frac{z_\pm F}{RT}\varphi_{\mathrm{EDL}}}\right) = \nabla \cdot \left[\mathcal{D}_\pm e^{-\frac{z_\pm F}{RT}\varphi_{\mathrm{EDL}}}\left(\nabla c_\mathrm{b} + \frac{z_\pm F}{RT} c_\mathrm{b} \nabla \varphi_\mathrm{b}\right)\right], \quad \mathbf{x} \in \mathcal{P} \tag{8a}$$

subject to the boundary conditions

$$\mathbf{n} \cdot \left(\nabla c_\mathrm{b} + \frac{z_\pm F}{RT} c_\mathrm{b} \nabla \varphi_\mathrm{b}\right) = 0, \quad \mathbf{x} \in \Gamma. \tag{8b}$$

Substituting Eqs. 5 and 7 into Eqs. 2 and 3, while accounting for Eq. 6, leads to a Poisson-Boltzmann equation

$$-\nabla^2\varphi_{\mathrm{EDL}} = \frac{F}{\mathcal{E}} c_\mathrm{b}\left(\nu_+ z_+ e^{-\frac{z_+ F}{RT}\varphi_{\mathrm{EDL}}} + \nu_- z_- e^{-\frac{z_- F}{RT}\varphi_{\mathrm{EDL}}}\right), \quad \mathbf{x} \in \mathcal{P} \tag{9a}$$

subject to the boundary condition

$$\varphi_{\mathrm{EDL}} = \varphi_\Gamma, \qquad \mathbf{x} \in \Gamma. \tag{9b}$$

This formulation of the PNP equations we proposed in Ref. 28 and subsequently used to upscale fluid flow in clays.[18–20]

To simplify the presentation, we set $\mathcal{D}_- = \mathcal{D}_+ \equiv \mathcal{D}$ and consider symmetric completely dissociated electrolyte ions, i.e., assume the equality of the ion charges (valency), $z_+ = -z_- \equiv z$, and dissociation constants, $\nu_+ = \nu_- \equiv \nu$. However, the methodology developed

below is equally applicable to multicomponent and/or asymmetric electrolytes.

Non-dimensional formulation.—The subsequent analysis is facilitated by introducing, in addition to $\epsilon = l/L$, dimensionless variables

$$\hat{\mathbf{x}} = \frac{\mathbf{x}}{L}, \quad \hat{t} = \frac{t\mathcal{D}}{L^2}, \quad \hat{\nabla} = L\nabla, \quad \hat{c}_\mathrm{b} = \frac{c_\mathrm{b}}{c_\mathrm{in}}, \quad \hat{\varphi} = \frac{F\varphi}{RT}, \quad [10]$$

where c_in is the initial ion concentration, and rewriting Eqs. 11a and 12 in dimensionless form:

$$\frac{\partial}{\partial \hat{t}}(\hat{c}_\mathrm{b} e^{\mp z\hat{\varphi}_\mathrm{EDL}}) = \hat{\nabla}\cdot\left[e^{\mp z\hat{\varphi}_\mathrm{EDL}}(\hat{\nabla}\hat{c}_\mathrm{b} \pm z\hat{c}_\mathrm{b}\hat{\nabla}\hat{\varphi}_\mathrm{b})\right], \quad \hat{\mathbf{x}} \in \hat{\mathcal{P}} \quad [11a]$$

subject to the boundary conditions

$$\hat{\mathbf{n}}\cdot(\hat{\nabla}\hat{c}_\mathrm{b} \pm z\hat{c}_\mathrm{b}\hat{\nabla}\hat{\varphi}_\mathrm{b}) = 0, \quad \hat{\mathbf{x}} \in \hat{\Gamma}; \quad [11b]$$

and

$$\epsilon^2\hat{\nabla}^2\hat{\varphi}_\mathrm{EDL} = \frac{l^2}{\lambda_\mathrm{D}^2}\hat{c}_\mathrm{b}\sinh(z\hat{\varphi}_\mathrm{EDL}), \quad \lambda_\mathrm{D} = \sqrt{\frac{RT\mathcal{E}}{2F^2 z\nu c_\mathrm{in}}}; \quad \hat{\mathbf{x}} \in \hat{\mathcal{P}} \quad [12a]$$

subject to the boundary condition

$$\hat{\varphi}_\mathrm{EDL} = \hat{\varphi}_\Gamma, \quad \hat{\mathbf{x}} \in \hat{\Gamma}. \quad [12b]$$

In nanoporous materials the Debye length λ_D, a characteristic length of the EDL, is of the same order of magnitude as the characteristic pore size l.

Macroscopic transport model.—Macroscopic representations of the nanoporous material Ω treat it as a continuum, without separating it into the pore space $\mathcal{P}$ and the solid skeleton $\mathcal{S}$. In other words, macroscopic ion concentration $C(\mathbf{x}, t)$ and electric potential $\Phi(\mathbf{x}, t)$ are defined at every "point" $\mathbf{x} \in \Omega$. One macroscopic characteristic of such a material is its porosity, $\omega = \|\mathcal{P}\|/\|\Omega\|$. Our goal is to estimate more elusive macroscopic properties, such as an effective diffusion coefficient, which are properties of both a nanoporous material and an electrolyte.

We use the multiple-scale expansion technique[10,29–31] to derive effective (macroscopic) counterparts of the PNP Equations 11 and 12. The method explicitly accounts for the spatial variability of ion concentration, and other dependent variables, on both macroscopic scale (across the porous material, denoted by the coordinate $\mathbf{x}$) and microscopic scale (inside individual pores, denoted by the coordinate $\mathbf{y}$). We assume that the bulk concentration and potential exhibit pronounced variability on both scales, i.e., $c_\mathrm{b} = c_\mathrm{b}(\mathbf{x}, \mathbf{y}, t)$ and $\varphi_\mathrm{b} = \varphi_\mathrm{b}(\mathbf{x}, \mathbf{y}, t)$; while the spatial variability of the EDL potential is confined to the nanoscale, i.e., $\varphi_\mathrm{EDL} = \varphi_\mathrm{EDL}(\mathbf{y}, t)$.

The latter assumption enables one to decouple Eqs. 11 and 12, and to compute $\varphi_\mathrm{EDL}(\mathbf{y})$ by solving Eq. 12 on a "unit cell" $\mathcal{U}$ representative of the material's pore structure,

$$\hat{\nabla}^2\hat{\varphi}_\mathrm{EDL} = \frac{l^2\hat{c}_\mathrm{b}^\star}{\epsilon^2\lambda_\mathrm{D}^2}\sinh(z\hat{\varphi}_\mathrm{EDL}), \quad \hat{\mathbf{y}} \in \hat{\mathcal{P}}_\mathcal{U}; \qquad \hat{\varphi}_\mathrm{EDL} = \hat{\varphi}_\Gamma, \quad \hat{\mathbf{x}} \in \hat{\Gamma}_\mathcal{U} \quad [13]$$

where $c_\mathrm{b}^\star$ is a characteristic ion concentration in the system, e.g., its initial or average value; and $\hat{\mathcal{P}}_\mathcal{U}$ and $\hat{\Gamma}_\mathcal{U}$ are the pore space and fluid-solid interface contained in the unit cell $\mathcal{U}$. Then, Eq. 11 is upscaled in Appendix A to yield continuum-scale Nernst-Planck equations satisfied by macroscopic ion concentration $C(\mathbf{x}, t)$ and electric potential $\Phi(\mathbf{x}, t)$,

$$\omega\frac{\partial C}{\partial t} = \nabla\cdot\left[\mathbf{D}_\pm^\mathrm{eff}\left(\nabla C \pm \frac{zF}{RT}C\nabla\Phi\right)\right]. \quad [14]$$

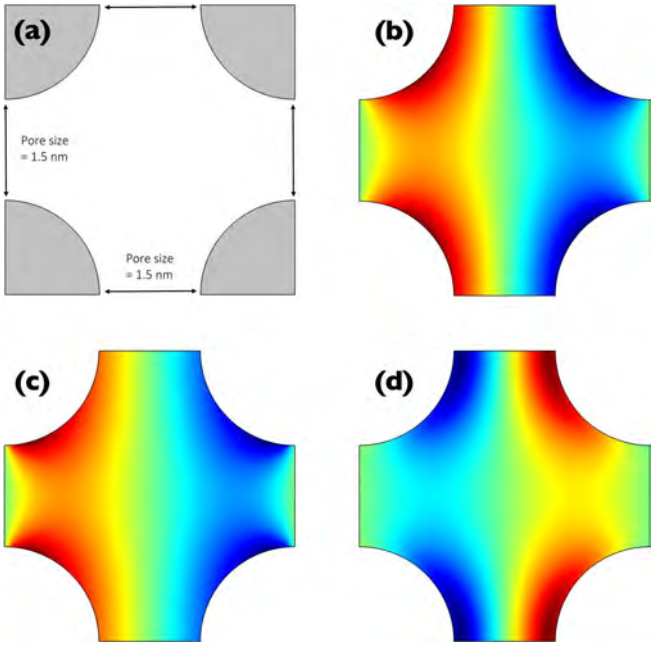

Figure 1. (a) A unit cell comprising a homogeneous isotropic nanoporous material with porosity $\omega = 0.67$ and pore throat size 1.5 nm. (b) Spatial distribution of the closure variable $\chi(y_1, y_2)$ for electroneutral fluid, computed by solving the scalar version of 16 with $\varphi_\mathrm{EDL} = 0$ for $c_\mathrm{in} = 0.93$ M. (c) and (d) Spatial distributions of the closure variables $\chi_+(y_1, y_2)$ and $\chi_-(y_1, y_2)$, respectively, computed by solving the scalar versions of 16 with $\varphi_\mathrm{EDL} = 0.3$ V for $c_\mathrm{in} = 0.93$ M.

Here the effective diffusion coefficients $\mathbf{D}_\pm^\mathrm{eff}$ are second-order semi-positive-definite tensors defined by

$$\mathbf{D}_\pm^\mathrm{eff} = \frac{\mathcal{D}\omega}{G_\pm}\int_{\hat{\mathcal{P}}_\mathcal{U}} e^{\mp z\hat{\varphi}_\mathrm{EDL}}(\mathbf{I} + \nabla_\mathbf{y}\boldsymbol{\chi}_\pm^\top)\mathrm{d}\mathbf{y}, \quad G_\pm = \int_{\hat{\mathcal{P}}_\mathcal{U}} e^{\mp z\hat{\varphi}_\mathrm{EDL}}\mathrm{d}\mathbf{y}, \quad [15]$$

where $\mathbf{I}$ is the identity matrix, and the closure variables $\boldsymbol{\chi}_\pm(\mathbf{y})$ are $\mathcal{U}$-periodic vector functions, which are computed as solutions of boundary-value problems

$$\begin{aligned}\nabla_\mathbf{y}[e^{\mp z\hat{\varphi}_\mathrm{EDL}}(\mathbf{I} + \nabla_\mathbf{y}\boldsymbol{\chi}_\pm^\top)] &= \mathbf{0}, \quad \mathbf{y} \in \hat{\mathcal{P}}_\mathcal{U};\\ \mathbf{n}(\mathbf{I} + \nabla_\mathbf{y}\boldsymbol{\chi}_\pm{}^\top) &= \mathbf{0}, \quad \mathbf{y} \in \hat{\Gamma}_\mathcal{U};\\ \int_{\hat{\mathcal{P}}_\mathcal{U}} \boldsymbol{\chi}_\pm\mathrm{d}\mathbf{y} &= \mathbf{0}.\end{aligned} \quad [16]$$

A few observations about this general result are in order. First, the effective Equations 14 are identical to those obtained phenomenologically from the solute material balance considerations[6]. Second, the rigorous derivation of these equations enables one to express the diffusion coefficient tensor in Eq. 15 in terms of the pore structure and electrical double layer potential, as opposed to treating them as fitting parameters. Third, it follows from Eq. 16 that the off-diagonal elements of the second-rank tensor $\nabla_\mathbf{y}\boldsymbol{\chi}_\pm^\top$ are zeros, i.e., $\partial\chi_{\pm,i}/\partial y_k = 0$ for $i \neq k$. Consequently, the off-diagonal elements of the diffusion tensors $\mathbf{D}_\pm^\mathrm{eff}$ are zero as well.

By way of example, let us consider a homogeneous isotropic nanoporous material assembled from the unit cell shown in Figure 1a. The unit cell's symmetry suggests that $\chi_{\pm,1} = \chi_{\pm,2}$, i.e., $\boldsymbol{\chi}_\pm(\mathbf{y}) = \chi_\pm(\mathbf{y})(1, 1)^\top$. The resulting isotropy of the nanoporous material implies that the diffusion coefficients in Eq. 15 become scalars, D_+^eff and D_-^eff. Figure 1b exhibits $\chi(\mathbf{y})$, a solution of the unit cell problem 16 with $\varphi_\Gamma = 0$ and, hence, $\varphi_\mathrm{EDL} = 0$, in the absence of electrical charge on the fluid-solid interface Γ. For charged surfaces ($\varphi_\Gamma = 0.3$ V), solutions for the closure variables $\chi_+(y_1, y_2)$ and

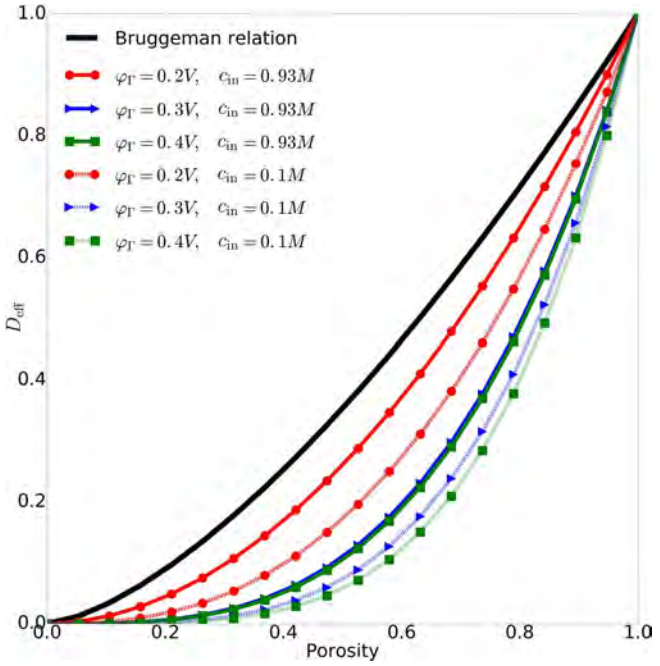

Figure 2. The normalized effective diffusion coefficient of an isotropic nanoporous material, $\mathcal{D}^{\text{eff}}/D$, computed alternatively with Bruggeman's relation $\mathcal{D}^{\text{eff}} = D\omega^{3/2}$ and our model 15 and 17. Unlike Bruggeman's relation, our model captures the dependence of D^{eff} on electrical surface potential φ_Γ and initial ion concentration c_{in}.

$\chi_-(y_1, y_2)$ are shown in Figures 1c and 1d, respectively. These three solutions demonstrate that the double layer potential φ_{EDL} affects the effective transport properties of nanoporous materials (the size of the pore throats in this example is 1.5 nm).

This finding is in contrast with often used phenomenological relations such as $\mathcal{D}^{\text{eff}} = \omega D/\tau$, where τ is the tortuosity of a porous medium, which is set to $\tau = \omega^{-0.5}$ in the Bruggeman model[6]. Such expressions are not readily adaptable to anisotropic materials and do not account for EDL's presence in charged nanoporous materials and, hence, for the dependence of $\mathcal{D}^{\text{eff}}$ on applied voltage. Figure 2 shows the dependence of the normalized effective diffusion coefficient $\mathcal{D}^{\text{eff}}/D$ on porosity ω, predicted with both Bruggeman's relation, $\mathcal{D}^{\text{eff}} = D\omega^{3/2}$, and the weighted harmonic mean (a binary effective diffusion coefficient[6]),

$$\mathcal{D}^{\text{eff}} = \frac{2D_+^{\text{eff}} D_-^{\text{eff}}}{D_+^{\text{eff}} + D_-^{\text{eff}}}, \qquad [17]$$

of the effective diffusion coefficients D_-^{eff} and D_+^{eff} computed with Eq. 15. As expected, the discrepancy between the two predictions increases with the surface potential φ_Γ.

The effective model presented above also allows one to estimate an electrode's surface potential φ_Γ, which is generated by applying an external voltage V. This is done by inverting a relationship[32]

$$\varphi_\Gamma = \frac{V}{2} - \varphi_{\text{ecm}} - \frac{\sigma}{C_{\text{H}}}, \qquad [18]$$

where φ_{ecm} is the electrocapillary maximum, C_{H} is the Helmholtz capacitance, and σ is the surface charge density. The electrocapillary maximum φ_{ecm} determines a material's resistance to applied voltage, i.e., the applied electrical driving force that has to be exceeded for electrosorption to set in; experiments on carbon aerogel electrodes[27] showed that $0.1\,\text{V} \le \varphi_{\text{ecm}} \le 0.25\,\text{V}$. For a dilute solution and low applied voltage 1.2 V, the Helmholtz capacitance C_{H} is practically independent of both the surface potential and electrolyte concentration[27,33] and has values[34] ranging from 20 μF/cm^2 to 45 μF/cm^2. Finally, the

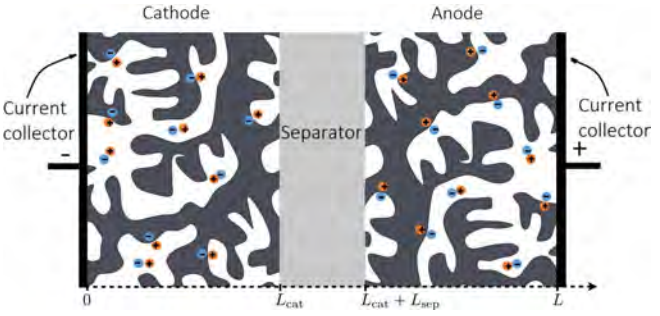

Figure 3. Schematic representation of an electrical double layer capacitor (EDLC) cell. Pore space of the cathode and anode and the separator is filled with electrolyte. The electrolyte within the carbon electrodes is electrically neutral, i.e., the total charge of the ions adsorbed on the electrode surfaces is balanced by the surface charge on the carbon electrodes. The separator is made of a porous dielectric material, such as glass fiber.

surface charge density σ is computed as[6,27,32]

$$\sigma = \sqrt{4\mathcal{E}RTI}\sqrt{\cosh\left(\frac{e\varphi_\Gamma}{kT}\right) - \cosh\left(\frac{e\varphi_{\min}}{kT}\right)},$$
$$I = z^2 C, \quad \varphi_{\min} = \min_{\mathbf{y}\in\mathcal{U}_\mathcal{P}} \varphi_{\text{EDL}}(\mathbf{y}) \qquad [19]$$

where I is the ionic strength, $\varphi_{\min}$ is the midplane potential computed by solving Eq. 13. Combining Eqs. 18 and 19 gives a transcendental equation for φ_Γ, whose solution, depending on the choice of parameters, varies between 0.2 V and 0.4 V when the external voltage $V = 1.2$ V is applied.

Application to Electrical Double Layer Capacitors

Electrical double layer capacitors (EDLCs) store energy in the EDL; they have been shown to possess high power density and long reversible cycle life. These properties suggest that EDLCs can be used in electric and hybrid electric vehicles to offset the low charge/discharge of current in batteries, providing an acceleration boost. The performance of EDLCs has been analyzed with effective electrodiffusion models, which were validated with experimental data[23,35,36]. Our goal is to improve the predictive power of EDLC models by using our expressions for the effective diffusion coefficients.

A mathematical model of EDLCs.—A typical EDLC consists of three compartments, positive and negative electrodes separated by a porous dielectric material (Fig. 3), which are fully saturated with electrolyte. The models[6,23] assume that i) both the electrodes (made from a porous activated-carbon material) and the separator are homogeneous and isotropic, ii) temperature is uniform and constant throughout the EDLC, and iii) convection in the cell is negligible.

Under these assumptions, the EDLC behavior is characterized by three macroscopic state variables: electrolyte ionic concentration, $C(x,t)$; electrolyte potential, $\Phi(x,t)$; and electric potential of the solid phase, $\Phi_{\text{s}}(x,t)$. For the EDLC in Fig. 3, these variables satisfy a three-equation model[23] (see Appendix B for derivation),

$$\mathcal{C}_{\text{EDL}}\frac{\partial(\Phi_{\text{s}} - \Phi)}{\partial t} = \frac{\partial}{\partial x}\left(\sigma_{\text{s}}\frac{\partial \Phi_{\text{s}}}{\partial x}\right), \qquad [20]$$

$$\frac{\partial}{\partial x}\left(\sigma_{\text{s}}\frac{\partial \Phi_{\text{s}}}{\partial x} + \kappa^{\text{eff}}\frac{\partial \Phi}{\partial x} + \kappa^{\text{eff}}RT\frac{2t_+ - 1}{zF}\frac{\partial \ln C}{\partial x}\right) = 0, \qquad [21]$$

$$\omega\frac{\partial C}{\partial t} = \frac{\partial}{\partial x}\left(\mathcal{D}^{\text{eff}}\frac{\partial C}{\partial x}\right) - \alpha\frac{\partial(\Phi_{\text{s}} - \Phi)}{\partial t}, \qquad [22]$$

Table I. Parameter values used in the experimental study[23] of supercapacitors.

Parameter	Value	Units
Electrodes thickness, $L_{cat} = L_{an}$	50	μm
Separator thickness, L_{sep}	25	μm
Initial ion concentration, c_{in}	0.93	mol/l
Porosity of electrodes, ω	0.67	-
Porosity of separator, ω	0.6	-
Solid phase conductivity, σ_s	52.1	S/m
Tortuosity of separator, τ_{sep}	1.3	-
Charge number, z	1	-
Dissociation coefficient, ν	1	-
Charging current, i	36.4	A/m^2
Conductivity of electrolyte at c_{in}, κ	0.67	mS/cm
Molecular diffusion coefficient, D	4.312×10^{-5}	cm^2/s

that is defined for $x \in [0, L]$. Here the effective conductivity of the electrolyte, κ^{eff}, is given by

$$\kappa^{eff} = \nu z^2 \frac{F^2 c_{in}}{RT}(D_+^{eff} + D_-^{eff}); \qquad [23a]$$

the transference number t_+, the fraction of the current carried by cations, has the form

$$t_+ = \frac{D_+^{eff}}{D_+^{eff} + D_-^{eff}}; \qquad [23b]$$

σ_s is the electric conductivity of the solid phase, with $\sigma_s = 0$ in the dielectric separator ($L_{cat} < x < L_{cat} + L_{sep}$); the EDL capacitance $\mathcal{C}_{EDL}$ is absent in the dielectric separator ($\mathcal{C}_{EDL} = 0$ for $L_{cat} < x < L_{cat} + L_{sep}$); and

$$\alpha = \frac{\mathcal{C}_{EDL}}{\nu z F} \begin{cases} t_+ - 1 & 0 < x < L_{cat} \\ 0 & L_{cat} < x < L_{cat} + L_{sep} \\ t_+ & L_{cat} + L_{sep} < x < L. \end{cases} \qquad [23c]$$

Since $\sigma_s = 0$ for $L_{cat} < x < L_{cat} + L_{sep}$, it follows from Eq. 20 that in the separator $i_{liquid} = i$, i.e., the liquid-phase current i_{liquid} equals the total (externally applied) current i. Moreover, since the solid phase of the separator is dielectric, $\Phi_s = 0$ for $L_{cat} < x < L_{cat} + L_{sep}$.

The partial-differential Equations 20–22 are subject to the following boundary conditions.[23] Since the EDLC surface is impermeable to electrolyte and the current it carries,

$$\frac{\partial C}{\partial x} = 0, \qquad \frac{\partial \Phi}{\partial x} = 0 \qquad \text{at } x = 0, L; \qquad [24a]$$

with the second condition stemming from $i_{liquid} = 0$. Application of the external current i to the anode ($x = L$) gives rise to the boundary condition

$$\sigma_s \frac{\partial \Phi_s}{\partial x} = -i \qquad \text{at } x = L. \qquad [24b]$$

Finally, the (reference) electric potential at the cathode ($x = 0$) is set to

$$\Phi_s = 0 \qquad \text{at } x = 0. \qquad [24c]$$

The initial conditions are $\Phi(x, 0) = 0$, $\sigma_s \partial_x \Phi_s(x, 0) = -i$ and $C(x, 0) = c_{in}$.

An observable quantity, and the quantity of interest computed with Eqs. 20–24, is an EDLC's voltage response, $V_{cell}(L, t) \equiv \Phi_s(L, t) - \Phi_s(0, t) = \Phi_s(L, t)$, to charging with the constant current i.

Model parametrization.—The experimental study[23] of an EDLC's voltage response involves activated carbon electrodes, whose homogeneous, orderly aligned microstructure has average pore throat size of 1.5 nm, with porosity $\omega = 0.67$. These and other relevant parameter values from this experiment are collated in Table 1. The nearly equal solvated tetrafluoroborate anion and tetraethylammonium cation sizes in acetonitrile used in the experiment suggest the equality of their molecular diffusion coefficients, $D_+ = D_- = D$. The value of $D = 4.312 \times 10^{-5}$ cm^2/s was determined from measurements of the electrical conductivity of acetonitrile by using a free-electrolyte version of Eq. 23a, $D = RT\kappa/(2\nu z^2 F^2 c_{in})$. The EDL capacitance $\mathcal{C}_{EDL}$ serves as the only fitting parameter[23].

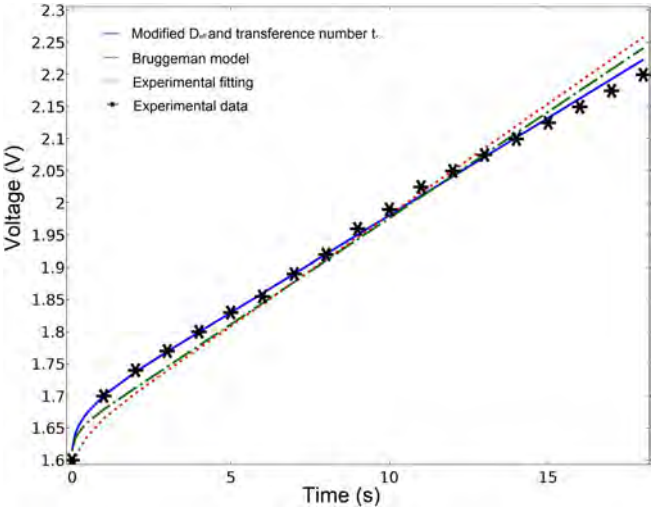

Figure 4. Measured EDLC voltage response to charging[23] (stars), and its counterparts predicted with the original model[23] (dotted line), the same model supplemented with the Bruggeman relation (dashed line) and our effective model (solid line).

Simulation results.—The parametrization of the mathematical model 20–24 in the analysis[23] is completed by employing the empirical relation $\mathcal{D}_\pm^{eff} = \mathcal{D}^{eff} = D\omega/\tau$ with an assumed tortuosity value of $\tau = 2.3$. According to Eq. 23, the equality $\mathcal{D}_+^{eff} = \mathcal{D}_-^{eff}$ translates into $t_+ = 0.5$ and $\kappa^{eff} = \kappa\omega/\tau$. Fitting the resulting model prediction of the EDLC voltage response to data yields $\mathcal{C}_{EDL} = 42$ F/cm^3, with the predicted voltage response $V_{cell}(t)$ shown in Figure 4 by the dotted line. A modification of this procedure, which replaces the assumed tortuosity value with that given by the Bruggeman relation $\tau = \omega^{-0.5} = 1.2$, yields $\mathcal{C}_{EDL} = 44$ F/cm^3 and the prediction of $V_{cell}(t)$ that is closer to the experiment (Fig. 4).

Unlike these two phenomenological relations, our model 15 yields unequal effective diffusion coefficients for cations and anions, $D_-^{eff} \neq D_+^{eff}$, which accounts for the EDL effects.[c] Substituting these values into Eqs. 23b and Eqs. 17 yields the cation (tetraethylamonium ion) transference number $t_+ = 0.779$ and the effective binary diffusion coefficient $\mathcal{D}^{eff}$, respectively. Fitting the resulting model prediction of the EDLC voltage response to data yields $\mathcal{C}_{EDL} = 47$ F/cm^3, with the predicted voltage response $V_{cell}(t)$ shown in Figure 4 by the solid line. This result demonstrates that our model matches the data better than its empirical counterparts; crucially, it does not rely on the assumed relation $\mathcal{D}^{eff} = D\omega/\tau$. (If needed, one can estimate an electrode's tortuosity from this relation, which for the material under investigation yields $\tau = \omega D/\mathcal{D}^{eff} = 2.4$ or $\tau = \omega^{-2.3}$).

Figure 5 exhibits temporal snapshots of the ion concentration and electric potential profiles computed alternatively with our rigorously derived model and the empirical Bruggeman relation. The system's nonlinearity magnifies the relatively minor errors in the

[c]These values were computed as follows. In the experiment[23], application of the constant charging current $i = 36.4$ A/m^2 to the anode changed the EDLC voltage from $V = 1.6$ V to $V = 2.2$ V (Fig. 4). We took the midpoint voltage as external voltage $V = 1.9$ V of EDLC cell during charging; from Eqs. 18 and 19, the diffuse layer potential $\varphi_\Gamma = 0.4$ V was calculated. Due to short charging time, the influence of concentration variation on EDL potential distribution is negligible. Double layer potential in Eq. 13 is thus solved with characteristic ion concentration $c_b^* = c_{in} = 0.93$ M and the diffuse layer potential $\varphi_\Gamma = 0.4$ V.

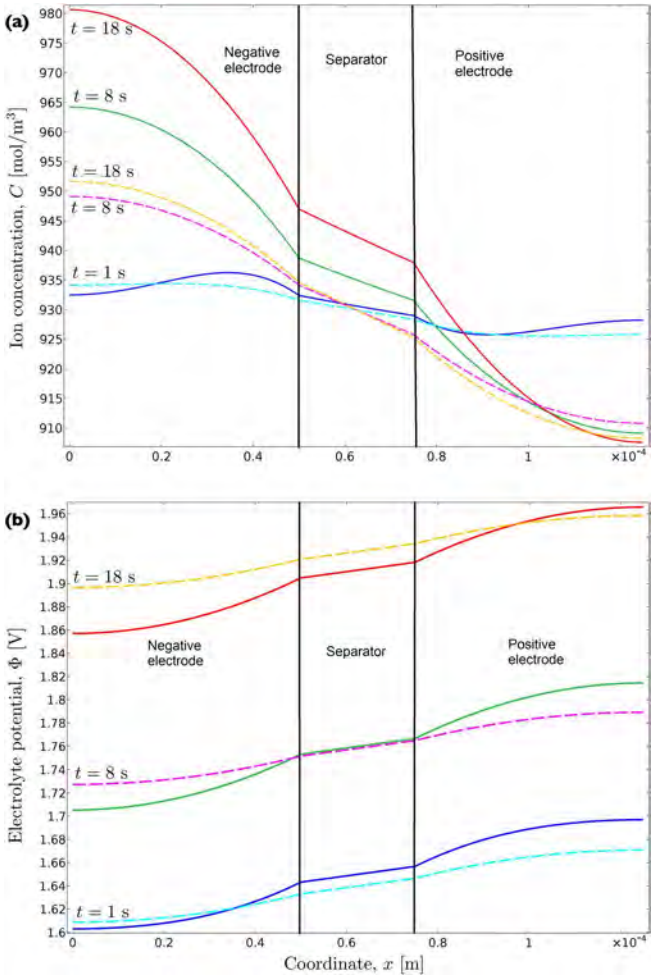

Figure 5. Temporal snapshots, at $t = 1, 8$ and 18 s, of the (a) ion concentration $C(x, t)$ and (b) electric potential $\Phi(x, t)$ profiles computed with our rigorously derived model (solid lines) and the Bruggeman relation (dashed lines). Our model predicts significantly higher gradients of both ion concentration and electric potential.

voltage-response predictions introduced by the Bruggeman relation (Fig. 4), resulting in the significant underestimation of the concentration and potential gradients (Fig. 5). Our model predicts the ion diffusion and electric conductivity coefficients that are smaller than their Bruggeman counterparts; consequently, the charge conservation in Eqs. 21 requires the significantly higher ion concentration and electric potential gradients to maintain sufficient amount of the ionic flux in electrolyte. The gradients of both the ion concentration and electric potential increase with time, as the EDLC continues to be charged with a constant current. At the early stage of charging ($t = 1$ s), the large electrolyte potential gradient in the vicinity of the separator (Fig. 5b) induces the non-monotonic spatial distribution of ion concentration (Fig. 5a). This behavior is due to the prescribed uniformity of the initial concentration, whose effect dissipates with time.

Conclusions

We derived expressions for effective diffusion coefficients $\mathbf{D}_{\pm}^{\text{eff}}$ and transference numbers $t_{\pm}$, which are used in macroscopic (continuum-scale) models of ion transport in nanoporous materials. These expressions relate the nanoscale topological properties of such materials (e.g., pore size and connectivity) to their macroscopic counterparts (e.g., porosity and tortuosity) and account for the nonlinear effects of the electrical double layer (EDL) on ion transport. While applicable to a wide range of electrochemical phenomena in porous materials, these expressions are deployed here to estimate the voltage response of an electrical double layer capacitor (EDLC) to charging. Our analysis leads to the following major conclusions.

(1) The effective diffusion coefficients $\mathbf{D}_{\pm}^{\text{eff}}$ are, in general, second-rank semi-positive definite tensors, reflecting possible anisotropy of nanoporous structures.
(2) Even if molecular diffusion coefficients of cations (D_+) and anions (D_-) in an electrolyte are equal, their effective counterparts differ, $\mathbf{D}_{+}^{\text{eff}} \neq \mathbf{D}_{-}^{\text{eff}}$, unless the binary electrolyte is symmetric (i.e., has equal dissociation coefficients, $\nu_+ = \nu_-$, and ion charges, $z_+ = z_-$).
(3) Even if the cations and anions in an electrolyte have similar size, their effective transference numbers are not equal, $t_+ \neq t_-$, unless the binary electrolyte is symmetric.
(4) These features of the effective parameters are a manifestation of the EDL's effects on diffusion of ions in nanoporous materials. These effects are not captured by phenomenological relations, such as Bruggeman's relation $D^{\text{eff}} = \omega^{3/2} D$, which estimate the effective ionic diffusion D^{eff} as a fraction of the molecular diffusion of ions in electrolyte, D, reduced by a power of porosity ω.
(5) Bruggeman's relation overestimates the effective diffusion coefficient and effective electric conductivity, especially for dilute solutions and relatively large diffuse layer potentials φ_Γ.
(6) By accounting for the electrochemical effect at the fluid-solid interfaces (specifically, the reduction of surface area[3]), our expressions increase the accuracy of predictions of double-layer capacitance of electrode materials.
(7) The use of our effective coefficients in a macroscopic model of EDLC charging yields the predictions of voltage response that are in close agreement with the data[23]. The reliance on Bruggeman's relation significantly underestimates the gradients of both ion concentration and electric potential within the EDLC.

In common with,[21,31,37,38] our analysis can also be used to establish the limits of applicability of the effective representation (models) of transport processes in porous media. Such descriptors typically break down for highly localized phenomena that give rise to high concentration gradients. The following assumptions are specific to our treatment of electrodiffusion in nanoporous materials. Reliance on the pore-scale Boltzmann equilibrium distribution in a binary dilute electrolyte implies that an ion is treated as a point charge and the EDL potential is approximated by the Poisson-Boltzmann equation. To account for ion-wall and ion-ion interactions due to a finite size of ions, one can deploy various approximations of the ion-ion correction function, such as hypernetted chain, Percus-Yevick or mean spherical approximations.[17,39]

Acknowledgment

This research was supported in part by the Defense Advanced Research Projects Agency under the EQUiPS program and the National Science Foundation under grant DMS-1522799.

Appendix A: Homogenization of PNP Equations

In the derivations below we drop the hats over the dimensionless quantities to simplify the notation. The "fast" ($\mathbf{y}$) and "slow" ($\mathbf{x}$) scales are related by $\mathbf{y} = \epsilon^{-1}\mathbf{x}$, with $\epsilon \ll 1$, such that $\nabla = \nabla_{\mathbf{x}} + \epsilon^{-1}\nabla_{\mathbf{y}}$. The state variables $c_{\text{b}}(\mathbf{x}, t)$ and $\varphi_{\text{b}}(\mathbf{x}, t)$ are replaced with their two-scale counterparts $c_{\text{b}}(\mathbf{x}, \mathbf{y}, t)$ and $\varphi_{\text{b}}(\mathbf{x}, \mathbf{y}, t)$, and the macroscopic (average) ion concentration and electric potential are defined as

$$C(\mathbf{x}, t) = \frac{\omega}{\|\mathcal{P}_{\mathcal{U}}\|} \int_{\mathcal{P}_{\mathcal{U}}} c_{\text{b}}(\mathbf{x}, \mathbf{y}, t) d\mathbf{y} \quad \text{and} \quad \Phi_{\text{av}}(\mathbf{x}, t) = \frac{\omega}{\|\mathcal{P}_{\mathcal{U}}\|} \int_{\mathcal{P}_{\mathcal{U}}} \varphi_{\text{b}}(\mathbf{x}, \mathbf{y}, t) d\mathbf{y}. \tag{A1}$$

Following the standard practice in homogenization, we postulate that the nanoporous material Ω can be viewed as an assemblage of periodically repeated unit cells $\mathcal{U}$, each of which consists of the fluid-filled pore space $\mathcal{P}_{\mathcal{U}}$ and solid phase $\mathcal{S}_{\mathcal{U}}$. Since $\varphi_{\text{EDL}} = \varphi_{\text{EDL}}(\mathbf{y})$,

$c_b = c_b(\mathbf{x}, \mathbf{y}, t)$ and $\varphi_b = \varphi_b(\mathbf{x}, \mathbf{y}, t)$, Eq. 11 yields

$$\begin{aligned} e^{\mp z\varphi_{EDL}} \frac{\partial c_b}{\partial t} &= e^{\mp z\varphi_{EDL}} \nabla_{\mathbf{x}} \cdot \{\nabla_{\mathbf{x}} c_b + \epsilon^{-1}\nabla_{\mathbf{y}} c_b \pm z c_b(\nabla_{\mathbf{x}}\varphi_b + \epsilon^{-1}\nabla_{\mathbf{y}}\varphi_b)\} \\ &\quad + \epsilon^{-1}\nabla_{\mathbf{y}} \cdot \{e^{\mp z\varphi_{EDL}}[\nabla_{\mathbf{x}} c_b + \epsilon^{-1}\nabla_{\mathbf{y}} c_b \\ &\quad \pm z c_b(\nabla_{\mathbf{x}}\varphi_b + \epsilon^{-1}\nabla_{\mathbf{y}}\varphi_b)]\}, \quad \mathbf{y} \in \mathcal{P}_{\mathcal{U}}. \end{aligned} \tag{A2a}$$

The interfacial condition 4 takes the form

$$\mathbf{n} \cdot \left[\nabla_{\mathbf{x}} c_b + \epsilon^{-1}\nabla_{\mathbf{y}} c_b \pm z c_b(\nabla_{\mathbf{x}}\varphi_b + \epsilon^{-1}\nabla_{\mathbf{y}}\varphi_b)\right] = 0, \quad \mathbf{y} \in \Gamma_{\mathcal{U}}. \tag{A2b}$$

Next, the state variables $c_b(\mathbf{x}, \mathbf{y}, t)$ and $\varphi_b(\mathbf{x}, \mathbf{y}, t)$ are expanded in asymptotic series in the powers of the small parameter ϵ,

$$c_b(\mathbf{x}, \mathbf{y}, t) = \sum_{m=0}^{\infty} \epsilon^m c_m(\mathbf{x}, \mathbf{y}, t), \qquad \varphi_b(\mathbf{x}, \mathbf{y}, t) = \sum_{m=0}^{\infty} \epsilon^m \varphi_m(\mathbf{x}, \mathbf{y}, t), \tag{A3}$$

where the functions $c_m(\mathbf{x}, \mathbf{y}, t)$ and $\varphi_m(\mathbf{x}, \mathbf{y}, t)$ are $\mathcal{U}$-periodic in $\mathbf{y}$. Substituting A3 into A2 and collecting the terms of equal powers of ϵ yields the following set of recursive boundary-value problems (BVPs) for the expansion coefficients c_i and φ_i $(i = 0, 1, \ldots)$.

Terms of order ϵ^{-2}.—Collecting the terms of order ϵ^{-2} yields

$$\nabla_{\mathbf{y}} \cdot [\Pi c_0 e^{\mp z\varphi_{EDL}}(\nabla_{\mathbf{y}} c_0 \pm z c_0 \nabla_{\mathbf{y}}\varphi_0)] = 0, \quad \mathbf{y} \in \mathcal{P}_{\mathcal{U}} \tag{A4a}$$

subject to

$$\mathbf{n} \cdot (\nabla_{\mathbf{y}} c_0 \pm z c_0 \nabla_{\mathbf{y}}\varphi_0) = 0, \quad \mathbf{y} \in \Gamma_{\mathcal{U}}. \tag{A4b}$$

This homogeneous BVP has a trivial solution, i.e., both c_0 and φ_0 are independent of $\mathbf{y}$. That indicates insignificant spatial variability of both bulk concentration and bulk potential at the pore scale.

Terms of order ϵ^{-1}.—Since c_0 and φ_0 are independent of $\mathbf{y}$, collecting the terms of order ϵ^{-1} yields

$$\nabla_{\mathbf{y}} \cdot [e^{\mp z\varphi_{EDL}} \nabla_{\mathbf{y}}(c_1 \pm z c_0 \varphi_1)] = -\nabla_{\mathbf{y}} e^{\mp z\varphi_{EDL}} \cdot (\nabla_{\mathbf{x}} c_0 \pm z c_0 \nabla_{\mathbf{x}}\varphi_0), \quad \mathbf{y} \in \mathcal{P}_{\mathcal{U}} \tag{A5a}$$

subject to

$$\mathbf{n} \cdot \nabla_{\mathbf{y}}(c_1 \pm z c_0 \varphi_1) = -\mathbf{n} \cdot (\nabla_{\mathbf{x}} c_0 \pm z c_0 \nabla_{\mathbf{x}}\varphi_0), \quad \mathbf{y} \in \Gamma_{\mathcal{U}}. \tag{A5b}$$

This BVP involves both the fast and slow scales; to decouple these scales we introduce pore-scale $\mathcal{U}$-periodic closure variables[14,18–20] $\boldsymbol{\chi}_{\pm}(\mathbf{y})$, such that

$$c_1 \pm z c_0 \varphi_1 = \boldsymbol{\chi}_{\pm} \cdot (\nabla_{\mathbf{x}} c_0 \pm z c_0 \nabla_{\mathbf{x}}\varphi_0). \tag{A6}$$

Substituting this closure approximation into A5 gives

$$\nabla_{\mathbf{y}} \cdot [e^{\mp z\varphi_{EDL}}(\mathbf{I} + \nabla_{\mathbf{y}}\boldsymbol{\chi}_{\pm}^{\top})(\nabla_{\mathbf{x}} c_0 \pm z c_0 \nabla_{\mathbf{x}}\varphi_0)] = 0, \quad \mathbf{y} \in \mathcal{P}_{\mathcal{U}} \tag{A7a}$$

subject to the boundary condition

$$-\mathbf{n} \cdot [(\mathbf{I} + \nabla_{\mathbf{y}}\boldsymbol{\chi}_{\pm}^{\top})(\nabla_{\mathbf{x}} c_0 \pm z c_0 \nabla_{\mathbf{x}}\varphi_0)] = 0, \quad \mathbf{y} \in \Gamma_{\mathcal{U}}. \tag{A7b}$$

These BVPs are turned into identities if the vector functions $\boldsymbol{\chi}_{\pm}^{\top}(\mathbf{y})$ are defined as solutions to the first two equations in 16. When supplemented with the third condition in 16, this definition ensures that a solution of the unit cell problem, i.e., the vector functions $\boldsymbol{\chi}_{\pm}^{\top}(\mathbf{y})$, is unique.[40–43]

Terms of order ϵ^{0}.—Collecting the terms of order ϵ^{0} yields

$$\begin{aligned} e^{\mp z\varphi_{EDL}} \frac{\partial c_0}{\partial t} &= e^{\mp z\varphi_{EDL}} \nabla_{\mathbf{x}} \cdot \{\nabla_{\mathbf{x}} c_0 + \nabla_{\mathbf{y}} c_1 \pm z c_0(\nabla_{\mathbf{x}}\varphi_0 + \nabla_{\mathbf{y}}\varphi_1)\} \\ &\quad + \nabla_{\mathbf{y}} \cdot \{e^{\mp z\varphi_{EDL}}[\nabla_{\mathbf{x}} c_1 + \nabla_{\mathbf{y}} c_2 \pm z c_0(\nabla_{\mathbf{x}}\varphi_1 + \nabla_{\mathbf{y}}\varphi_2) \\ &\quad \pm z c_1(\nabla_{\mathbf{x}}\varphi_0 + \nabla_{\mathbf{y}}\varphi_1)]\}, \quad \mathbf{y} \in \mathcal{P}_{\mathcal{U}} \end{aligned} \tag{A8a}$$

subject to

$$\mathbf{n} \cdot [\nabla_{\mathbf{x}} c_1 + \nabla_{\mathbf{y}} c_2 \pm z c_0(\nabla_{\mathbf{x}}\varphi_1 + \nabla_{\mathbf{y}}\varphi_2) \pm z c_1(\nabla_{\mathbf{x}}\varphi_0 + \nabla_{\mathbf{y}}\varphi_1)] = 0, \quad \mathbf{y} \in \Gamma_{\mathcal{U}}. \tag{A8b}$$

Approximating c_b and φ_b in A1 with their leading-order counterparts, c_0 and φ_0, and integrating A8a over $\mathcal{P}_{\mathcal{U}}$ leads to

$$\frac{\partial C}{\partial t} = \nabla_{\mathbf{x}} \cdot \left[\nabla_{\mathbf{x}} C \pm \frac{zC}{\omega}\nabla_{\mathbf{x}}\Phi_{av} + \frac{\omega}{G_{\pm}\|\mathcal{P}_{\mathcal{U}}\|}\int_{\mathcal{P}_{\mathcal{U}}} e^{\mp z\varphi_{EDL}} \nabla_{\mathbf{y}}(c_1 \pm z c_0 \varphi_1) d\mathbf{y}\right], \tag{A9}$$

where $G_{\pm}$ is defined in Eq. 15. Accounting for A6, this turns into

$$\frac{\partial C}{\partial t} = \nabla_{\mathbf{x}} \cdot \left[\left(\mathbf{I} + \frac{1}{G_{\pm}}\int_{\mathcal{P}_{\mathcal{U}}} e^{\mp z\varphi_{EDL}} \nabla_{\mathbf{y}}\boldsymbol{\chi}_{\pm}^{\top} d\mathbf{y}\right)\left(\nabla_{\mathbf{x}} C \pm \frac{zC}{\omega}\nabla_{\mathbf{x}}\Phi_{av}\right)\right]. \tag{A10}$$

To account for the effects of electrical potential in the solid matrix, it is common[6] to define an average potential for the fluid-solid mixture. In our context, it is equivalent to defining the average as $\Phi(\mathbf{x}, t) = \frac{1}{\|\mathcal{U}\|}\int_{\mathcal{P}_{\mathcal{U}}} \varphi_b(\mathbf{x}, \mathbf{y}, t) d\mathbf{y}$, i.e., setting $\Phi = \Phi_{av}/\omega$. This leads to Eq. 14 with the effective diffusion coefficient tensors $\mathbf{D}_{\pm}^{\text{eff}}$ given by Eq. 15.

The condition $\int_{\mathcal{P}_{\mathcal{U}}} \boldsymbol{\chi}_{\pm} d\mathbf{y} = 0$ also ensures the order (in ϵ) consistency between the approximations of the (dimensionless) bulk electrochemical potential $\hat{\mu}_{b\pm} = \ln \hat{c}_{b\pm} + z_{\pm}\hat{\varphi}_b$ and other state variables. Indeed, dropping the hats, substituting the expansions A3 into this expression and retaining the terms up to the second order in ϵ yields $\mu_{b\pm} = \ln c_0 \pm z\varphi_0 + \epsilon(c_1 \pm z c_0\varphi_1)/c_0 + \mathcal{O}(\epsilon^2)$. Accounting for the closure A6 this leads to $\mu_{b\pm} = \ln c_0 \pm z\varphi_0 + \epsilon\, \boldsymbol{\chi}_{\pm} \cdot \nabla_{\mathbf{x}}(\ln c_0 \pm z\varphi_0) + \mathcal{O}(\epsilon^2)$. Integration of this expression over $\mathcal{P}_{\mathcal{U}}$ yields the leading-order approximation of the average electrochemical potential in terms of the leading-order approximations of the average concentration and bulk potential.

Appendix B: Macroscopic Model of an EDLC Cell

Charge conservation.—Total electrical current through a porous electroconductive material, $\mathbf{i} = \mathbf{i}_{\text{solid}} + \mathbf{i}_{\text{liquid}}$, is the sum of the currents through its solid ($\mathbf{i}_{\text{solid}}$) and liquid-saturated ($\mathbf{i}_{\text{liquid}}$) phases. Hence, conservation of the total charge, $\nabla \cdot \mathbf{i} = 0$, yields

$$\nabla \cdot \mathbf{i}_{\text{liquid}} = -\nabla \cdot \mathbf{i}_{\text{solid}}. \tag{B1}$$

Because of electric double layer charging/discharging, the charges are stored in double layer capacitance. Conservation of charge in the liquid phase leads to[6]

$$\nabla \cdot \mathbf{i}_{\text{liquid}} = \mathcal{C}_{\text{EDL}} \frac{\partial(\Phi_s - \Phi)}{\partial t}, \tag{B2}$$

where $\mathcal{C}_{\text{EDL}}$ is the EDL capacitance [F/cm^3]. Substituting B1 into B2 and using Ohm's law in solid phase $\mathbf{i}_{\text{solid}} = -\sigma_s \nabla\Phi_s$, where σ_s is the electric conductivity of the solid phase [S/m], yields

$$\mathcal{C}_{\text{EDL}} \frac{\partial(\Phi_s - \Phi)}{\partial t} = \nabla \cdot (\sigma_s \nabla\Phi_s). \tag{B3}$$

Mass conservation.—Macroscopic mass balance (Nernst-Plank) equations for positively and negatively charged ions have the form

$$\omega \frac{\partial C_{\pm}}{\partial t} = -\nabla \cdot \mathbf{J}_{\text{NP}}^{\pm} + S_{\pm}, \quad \mathbf{J}_{\text{NP}}^{\pm} = -D_{\pm}^{\text{eff}} \nabla C_{\pm} - D_{\pm}^{\text{eff}} \frac{z_{\pm} F}{RT} C_{\pm} \nabla\Phi. \tag{B4}$$

The concentrations of cations (C_+) and anions (C_-) are related to the ion concentration C by

$$C = \frac{C_+}{\nu_+} = \frac{C_-}{\nu_-}, \tag{B5}$$

where $\nu_{\pm}$ are the dissociation coefficients. Combined with B5, the charge neutrality condition,[6] $F z_+ C_+ + F z_- C_- = 0$, gives

$$z_+\nu_+ + z_-\nu_- = 0. \tag{B6}$$

(For example, asymmetric electrolyte $CaCl_2$ has $\nu_+ = 1$ and $\nu_- = 2$, and the ion charges $z_+ = 2$ and $z_- = -1$.) The current density $S_{\pm}(\mathbf{x}, t)$ represents the rate of ion transfer to/from the EDL storage. We express it as

$$S_{\pm} = \mathcal{H}[\pm(\Phi - \Phi_s)]\mathcal{M} R_{\text{EDL}}, \tag{B7}$$

where $\mathcal{H}[\cdot]$ is the Heaviside function, $\mathcal{M}(\mathbf{x})$ is the membership function such that $\mathcal{M} = 1$ for all $\mathbf{x}$ in the electrodes and $= 0$ otherwise, and the transfer rate R_{EDL} is defined as follows. Multiplying B4 with $F z_{\pm}$ and summing up the resulting two equations, while accounting for B5 and B6, yields $\nabla \cdot \mathbf{i}_{\text{liquid}} = F(z_+ S_+ + z_- S_-)$; combining this with B2 and B7 gives an expression for the transfer rate,

$$\mathcal{M} R_{\text{EDL}} = \frac{\mathcal{C}_{\text{EDL}}}{\psi F} \frac{\partial(\Phi_s - \Phi)}{\partial t}, \tag{B8}$$

where $\psi = z_+ \mathcal{H}(\Phi - \Phi_s) + z_- \mathcal{H}(\Phi_s - \Phi)$.

Problem reformulation in terms of charge current.—The analyzes[6,23] found it necessary to rewrite conservation laws B4 and B1 in terms of the ionic flux $\mathbf{i}_{\text{liquid}} = F(z_+\mathbf{J}_{\text{NP}}^{+} + z_-\mathbf{J}_{\text{NP}}^{-})$. Substituting the definition of $\mathbf{J}_{\text{NP}}^{\pm}$ in B4 into this expression we obtain

$$\frac{\mathbf{i}_{\text{liquid}}}{\nu_+ z_+ F} = -\frac{F}{RT}\left(z_+ D_+^{\text{eff}} + \frac{\nu_- z_-^2}{\nu_+ z_+} D_-^{\text{eff}}\right) C \nabla\Phi - \left(D_+^{\text{eff}} + \frac{\nu_- z_-}{\nu_+ z_+} D_-^{\text{eff}}\right) \nabla C. \tag{B9}$$

Using the latter to eliminate $C\nabla\Phi$ from the definition of $\mathbf{J}_{\text{NP}}^{+}$ leads to

$$\mathbf{J}_{\text{NP}}^{+} = -\nu_+ \mathcal{D}_+^{\text{eff}} \nabla C + \frac{t_+ \mathbf{i}_{\text{liquid}}}{z_+ F}, \tag{B10}$$

with the binary effective diffusion coefficient $\mathcal{D}^{\text{eff}}$ and the transference number t_+ defined as

$$\mathcal{D}_+^{\text{eff}} = \frac{\nu_- z_-(z_- - z_+) D_+^{\text{eff}} D_-^{\text{eff}}}{\nu_+ z_+^2 D_+^{\text{eff}} + \nu_- z_-^2 D_-^{\text{eff}}}, \qquad t_+ = \frac{\nu_+ z_+^2 D_+^{\text{eff}}}{\nu_+ z_+^2 D_+^{\text{eff}} + \nu_- z_-^2 D_-^{\text{eff}}}. \tag{B11}$$

By the same token, eliminating $C\nabla\Phi$ from the definition of $\mathbf{J}_{\rm NP}^{-}$ yields

$$\mathbf{J}_{\rm NP}^{-} = -\nu_{-}\mathcal{D}_{-}^{\rm eff}\nabla C + \frac{t_{-}\mathbf{i}_{\rm liquid}}{z_{-}F} \qquad [B12]$$

with

$$\mathcal{D}_{-}^{\rm eff} = \frac{\nu_{+}z_{+}(z_{+}-z_{-})D_{+}^{\rm eff}D_{-}^{\rm eff}}{\nu_{+}z_{+}^{2}D_{+}^{\rm eff}+\nu_{-}z_{-}^{2}D_{-}^{\rm eff}}, \qquad t_{-} = \frac{\nu_{-}z_{-}^{2}D_{-}^{\rm eff}}{\nu_{+}z_{+}^{2}D_{+}^{\rm eff}+\nu_{-}z_{-}^{2}D_{-}^{\rm eff}}. \qquad [B13]$$

Hence, we obtain a general expression for the ion fluxes

$$\mathbf{J}_{\rm NP}^{\pm} = -\nu_{\pm}\mathcal{D}_{\pm}^{\rm eff}\nabla C + \frac{t_{\pm}\mathbf{i}_{\rm liquid}}{z_{\pm}F}. \qquad [B14]$$

The charge conservation law B1 is rewritten[6,23] by combining it with Ohm's law, $\mathbf{i}_{\rm solid} = -\sigma_{\rm s}\nabla\Phi_{\rm s}$, the definition of the the ionic flux, $\mathbf{i}_{\rm liquid} = F(z_{+}\mathbf{J}_{\rm NP}^{+} + z_{-}\mathbf{J}_{\rm NP}^{-})$, and the definitions of $\mathbf{J}_{\rm NP}^{\pm}$ in Eq. B4:

$$\nabla\cdot(\kappa^{\rm eff}\nabla\Phi) + F\nabla\cdot[(\nu_{+}z_{+}\mathcal{D}_{+}^{\rm eff}+\nu_{-}z_{-}\mathcal{D}_{-}^{\rm eff})C\nabla\ln C) = -\nabla\cdot(\sigma_{\rm s}\nabla\Phi_{\rm s}), \qquad [B15]$$

where the effective conductivity of the electrolyte is defined as

$$\kappa^{\rm eff} = \frac{F^{2}C}{RT}(\nu_{+}z_{+}^{2}\mathcal{D}_{+}^{\rm eff}+\nu_{-}z_{-}^{2}\mathcal{D}_{-}^{\rm eff}). \qquad [B16]$$

When combined with the expressions for the transference numbers t_{+} and t_{-} in Eqs. B11 and B13, this definition of $\kappa^{\rm eff}$ transforms B15 into

$$\nabla\cdot\left[\kappa^{\rm eff}\nabla\Phi + \kappa^{\rm eff}\frac{RT}{F}\left(\frac{t_{+}}{z_{+}}+\frac{t_{-}}{z_{-}}\right)\nabla\ln C\right] = -\nabla\cdot(\sigma_{\rm s}\nabla\Phi_{\rm s}). \qquad [B17]$$

A three-compartment formulation.—The mass conservation Equations B4 and B14 are simplified when written for each compartment (the two electrodes and separator in Fig. 3 separately. In the cathode ($0 < x < L_{\rm cat}$), $\Phi - \Phi_{\rm s} > 0$ and combining B4, B7, B8 and B14 yields mass conservation equations

$$\omega\frac{\partial C}{\partial t} = \nabla\cdot(\mathcal{D}_{+}^{\rm eff}\nabla C) + \frac{t_{-}\mathcal{C}_{\rm EDL}}{\nu_{+}z_{+}F}\frac{\partial(\Phi_{\rm s}-\Phi)}{\partial t} \qquad [B18a]$$

and

$$\omega\frac{\partial C}{\partial t} = \nabla\cdot(\mathcal{D}_{-}^{\rm eff}\nabla C) - \frac{t_{-}\mathcal{C}_{\rm EDL}}{\nu_{-}z_{-}F}\frac{\partial(\Phi_{\rm s}-\Phi)}{\partial t}. \qquad [B18b]$$

These two equations are identical since, accounting for Eq. B6, $\mathcal{D}_{+}^{\rm eff} = \mathcal{D}_{-}^{\rm eff} \equiv \mathcal{D}^{\rm eff}$. A similar procedure is used to derive mass conservation equations for the anode ($L_{\rm cat}+L_{\rm sep} < x < L$), wherein $\Phi - \Phi_{\rm s} < 0$. Finally, mass conservation equations for the separator ($L_{\rm cat} < x < L_{\rm sep}$) are derived by setting $S_{\pm} = 0$. The resulting mass balance equation takes the form

$$\omega\frac{\partial C}{\partial t} = \nabla\cdot(\mathcal{D}^{\rm eff}\nabla C) - \alpha\frac{\partial(\Phi_{\rm s}-\Phi)}{\partial t}, \quad 0 < x < L; \qquad [B19a]$$

where

$$\alpha = \begin{cases} \frac{t_{-}\mathcal{C}_{\rm EDL}}{z_{-}\nu_{-}F} & 0 < x < L_{\rm cat} \\ 0 & L_{\rm cat} < x < L_{\rm cat}+L_{\rm sep} \\ \frac{t_{+}\mathcal{C}_{\rm EDL}}{z_{+}\nu_{+}F} & L_{\rm cat}+L_{\rm sep} < x < L. \end{cases} \qquad [B19b]$$

The three conservation Equations, B3, B17 and B19, govern the dynamics of the three state variables, $C(\mathbf{x},t)$, $\Phi(\mathbf{x},t)$ and $\Phi_{\rm s}(\mathbf{x},t)$. These equations are subject to boundary conditions at the EDLC external surfaces $x = 0$ and $x = L$. When solved separately in each of the compartments, they are also subject to continuity conditions at the internal interfaces $x = L_{\rm cat}$ and $x = L_{\rm cat}+L_{\rm sep}$.[23]

Model simplification for symmetric binary electrolytes.—These equations are simplified for a symmetric binary electrolyte ($\nu_{+} = \nu_{-} \equiv \nu$) with equal of ion charges ($z_{+} = -z_{-} \equiv z$). In this case, both $\mathcal{D}_{+}^{\rm eff}$ in B11 and $\mathcal{D}_{-}^{\rm eff}$ in B13 reduce to $\mathcal{D}^{\rm eff}$ given by Eq. 17, t_{+} in B11 gives rise to its counterpart in Eq. 23b, t_{-} in B13 becomes $t_{-} = 1 - t_{+}$, and $\kappa^{\rm eff}$ in B16 is approximated with Eq. 23a upon replacing the ion concentration C with its initial value $c_{\rm in}$. Finally, the governing Equations B3, B17 and B19 reduce to their one-dimensional counterparts 20, 21 and 22.

References

1. S. T. Mayer, R. W. Pekala, and J. L. Kaschmitter, "The aerocapacitor: An electrochemical double-layer energy-storage device," *J. Electrochem. Soc.*, **140**(2), 446 (1993).
2. I. Bispo-Fonseca, J. Aggar, C. Sarrazin, P. Simon, and J. F. Fauvarque, "Possible improvements in making carbon electrodes for organic supercapacitors," *J. Power Sources*, **79**(2), 238 (1999).
3. B. E. Conway, *Electrochemical supercapacitors: scientific fundamentals and technological applications*. Springer, 2013.
4. J. Chmiola, G. Yushin, Y. Gogotsi, C. Portet, P. Simon, and P. L. Taberna, "Anomalous increase in carbon capacitance at pore sizes less than 1 nanometer," *Science*, **313**(5794), 1760 (2006).
5. A. Soffer and M. Folman, "The electrical double layer of high surface porous carbon electrode," *J. Electroanal. Chem. Interfacial Electrochem.*, **38**(1), 25 (1972).
6. J. Newman and K. E. Thomas-Alyea, *Electrochemical Systems*. John Wiley & Sons, 2012.
7. R. Narayanan, H. Vijwani, S. M. Mukhopadhyay, and P. R. Bandaru, "Electrochemical charge storage in hierarchical carbon manifolds," *Carbon*, **99**, 267 (2016).
8. D.-W. Wang, F. Li, M. Liu, G. Q. Lu, and H.-M. Cheng, "3D aperiodic hierarchical porous graphitic carbon material for high-rate electrochemical capacitive energy storage," *Angew. Chem*, **120**(2), 379 (2008).
9. G.-J. Lee and S.-I. Pyun, "Theoretical approach to ion penetration into pores with pore fractal characteristics during double-layer charging/discharging on a porous carbon electrode," *Langmuir*, **22**(25), 10659 (2006).
10. X. Zhang, K. Urita, I. Moriguchi, and D. M. Tartakovsky, "Design of nanoporous materials with optimal sorption capacity," *J. Appl. Phys.*, **117**(24), 244304 (2015).
11. D.-W. Chung, M. Ebner, D. R. Ely, V. Wood, and R. E. García, "Validity of the Bruggeman relation for porous electrodes," *Modelling Simul. Mater. Sci. Eng.*, **21**, 074009 (2013).
12. A. Gully, H. Liu, S. Srinivasan, A. K. Sethurajan, S. Schougaard, and B. Protas, "Effective transport properties of porous electrochemical materials–a homogenization approach," *J. Electrochem. Soc.*, **161**(8), E3066 (2014).
13. I. V. Thorat, D. E. Stephenson, N. A. Zacharias, K. Zaghib, J. N. Harb, and D. R. Wheeler, "Quantifying tortuosity in porous Li-ion battery materials," *J. Power Sources*, **188**(2), 592 (2009).
14. M. Schmuck and M. Z. Bazant, "Homogenization of the Poisson-Nernst-Planck equations for ion transport in charged porous media," *SIAM J. Appl. Math.*, **75**(3), 1369 (2015).
15. P. M. Biesheuvel and M. Z. Bazant, "Nonlinear dynamics of capacitive charging and desalination by porous electrodes," *Phys. Rev. E*, **81**(3), 031502 (2010).
16. J. R. Looker and S. L. Carnie, "Homogenization of the ionic transport equations in periodic porous media," *Transport Porous Med.*, **65**(1), 107 (2006).
17. T. D. Le, C. Moyne, and M. A. Murad, "A three-scale model for ionic solute transport in swelling clays incorporating ion–ion correlation effects," *Adv. Water Resour.*, **75**, 31 (2015).
18. M. A. Murad and C. Moyne, "A dual-porosity model for ionic solute transport in expansive clays," *Comput. Geosci.*, **12**(1), 47 (2008).
19. C. Moyne and M. A. Murad, "A two-scale model for coupled electro-chemo-mechanical phenomena and Onsager's reciprocity relations in expansive clays: I homogenization analysis," *Transport Porous Med.*, **62**(3), 333 (2006).
20. C. Moyne and M. A. Murad, "Electro-chemo-mechanical couplings in swelling clays derived from a micro/macro-homogenization procedure," *Int. J. Solids Struct.*, **39**(25), 6159 (2002).
21. H. Arunachalam, S. Onori, and I. Battiato, "On veracity of macroscopic lithium-ion battery models," *J. Electrochem. Soc.*, **162**(10), A1940 (2015).
22. C. Timofte, "Homogenization results for ionic transport in periodic porous media," *Comput. Math. Appl.*, **68**(9), 1024 (2014).
23. M. W. Verbrugge and P. Liu, "Microstructural analysis and mathematical modeling of electric double-layer supercapacitors," *J. Electrochem. Soc.*, **152**(5), D79 (2005).
24. R. D. Shannon, "Revised effective ionic radii and systematic studies of interatomic distances in halides and chalcogenides," *Acta Cryst.*, **A32**(5), 751 (1976).
25. G. Karniadakis, A. Beskok, and N. Aluru, *Microflows and nanoflows: fundamentals and simulation*, 29. Springer Science & Business Media, 2006.
26. B. J. Kirby, *Micro-and nanoscale fluid mechanics: transport in microfluidic devices*. Cambridge University Press, 2010.
27. K.-L. Yang, T.-Y. Ying, S. Yiacoumi, C. Tsouris, and E. S. Vittoratos, "Electrosorption of ions from aqueous solutions by carbon aerogel: an electrical double-layer model," *Langmuir*, **17**(6), 1961 (2001).
28. S. G. Bike and D. C. Prieve, "Electrohydrodynamics of thin double layers: a model for the streaming potential profile," *J. Colloid Interf. Sci.*, **154**(1), 87 (1992).
29. U. Hornung, *Homogenization and Porous Media*. New York: Springer, 1997.
30. J.-L. Auriault and J. Lewandowska, "Effective diffusion coefficient: from homogenization to experiment," *Transport Porous Med.*, **27**(2), 205 (1997).
31. I. Battiato and D. M. Tartakovsky, "Applicability regimes for macroscopic models of reactive transport in porous media," *J. Contam. Hydrol.*, **120–121**, 18 (2011).
32. R. J. Hunter, *Foundations of colloid science*. Oxford University Press, 2001.
33. J. Varghese, H. Wang, and L. Pilon, "Simulating electric double layer capacitance of mesoporous electrodes with cylindrical pores," *J. Electrochem. Soc.*, **158**(10), A1106 (2011).
34. D. C. Grahame, "Differential capacity of mercury in aqueous sodium fluoride solutions. I. Effect of concentration at 25°," *J. Am. Chem. Soc.*, **76**(19), 4819 (1954).
35. S. Allu, B. V. Asokan, W. A. Shelton, B. Philip, and S. Pannala, "A generalized multi-dimensional mathematical model for charging and discharging processes in a supercapacitor," *J. Power Sources*, **256**, 369 (2014).
36. A. G. Kashkooli, S. Farhad, V. Chabot, A. Yu, and Z. Chen, "Effects of structural design on the performance of electrical double layer capacitors," *Appl. Energ.*, **138**, 631 (2015).
37. I. Battiato, D. M. Tartakovsky, A. M. Tartakovsky, and T. Scheibe, "On breakdown of macroscopic models of mixing-controlled heterogeneous reactions in porous media," *Adv. Water Resour.*, **32**, 1664 (2009).
38. F. Boso and I. Battiato, "Homogenizability conditions for multicomponent reactive transport," *Adv. Water Resour.*, **62**(Part B), 254 (2013).
39. D. A. McQuarrie, *Statistical Mechanics*. Sausalito, CA: University Science Books, 2000.

40. J.-L. Auriault, C. Boutin, and C. Geindreau, *Homogenization of coupled phenomena in heterogenous media*, 149. John Wiley & Sons, 2010.
41. G. A. Chechkin, A. L. Piatnitski, and A. S. Shamaev, *Homogenization*, 234 of *Translations of Mathematical Monographs*. Providence, RI: American Mathematical Society, 2007.
42. J. L. Auriault, "Heterogeneous media: is an equivalent homogeneous description always possible?," *Int. J. Engrg. Sci.*, **29**(7), 785 (1991).
43. J. L. Auriault and J. Lewandowska, "Homogenization analysis of diffusion and adsorption macrotransport in porous media: macrotransport in the absence of advection," *Geotechnique*, **43**(3), 457 (1993).